Comparison of the Complexes Formed by Cytochrome $P450_{cam}$ with Cytochrome b_5 and Putidaredoxin, Two Effectors of Camphor Hydroxylase Activity†

Lingyun Rui,‡ Susan Sondej Pochapsky,‡ and Thomas C. Pochapsky*,‡,§

Departments of Chemistry and Biochemistry, Brandeis University, 415 South Street, MS 015, Waltham, Massachusetts 02454-9110

Received November 11, 2005; Revised Manuscript Received January 19, 2006

ABSTRACT: Structural perturbations in cytochrome $P450_{cam}$ (CYP101) induced by the soluble fragment of cytochrome b_5, a nonphysiological effector of CYP101, were investigated by NMR spectroscopy and compared with the perturbations induced by the physiological reductant and effector putidaredoxin (Pdx). Chemical shifts of perdeuterated [U-^{15}N]CYP101 backbone amide (NH) resonances were monitored as a function of cytochrome b_5 concentration by ^{1}H−^{15}N TROSY-HSQC experiments. The association of cytochrome b_5 with the reduced CYP101−camphor−carbon monoxide complex (CYP−S−CO) perturbs many of the same resonances that Pdx does, including regions of the CYP101 molecule implicated in substrate access and orientation. The perturbations are smaller in magnitude than those observed with Pdx^r due to a lower binding affinity (a K_d of 13 ± 3 mM, for the reduced cytochrome b_5−CYP−S−CO complex compared to a K_d of 26 ± 12 μM for the Pdx−CYP−S−CO complex). The results are in accord with our previous suggestion that the observed perturbations are related to effector activity and support the proposal that the primary role of the effector is to populate the active conformation of CYP101 to prevent uncoupling [Pochapsky, S. S., et al. (2003) *Biochemistry 42,* 5649−5656]. A titratable perturbation is observed at the ^{1}H resonance of the 8-CH_3 group of CYP101-bound camphor upon addition of cytochrome b_5, a phenomenon also associated with the formation of the CYP101·Pdx complex, albeit with larger perturbations [Wei, J. Y., et al. (2005) *J. Am. Chem. Soc. 127,* 6974−6976]. The effector activity of the particular rat cytochrome b_5 construct used for NMR studies was confirmed by monitoring the enzymatic turnover that yielded 5-*exo*-hydroxycamphor using gas chromatography and mass spectrometry. Finally, the common features of the perturbations observed in the NMR spectra of the two complexes are discussed, and their relevance to effector activity is considered.

Cytochrome P450s are ubiquitous heme-thiolate enzymes that catalyze oxidative modifications of diverse substrates (*1*). Because of their central role in drug metabolism and involvement in steroid biosynthesis, cytochrome P450s are one of the most intensively investigated metalloenzymes (*2*). There are nearly 4000 identified P450 genes and structures for 20 unique P450s on deposit in the RCSB Protein Data Bank. The structurally and biochemically best-characterized cytochrome P450 is $P450_{cam}$ (CYP101)[1] from *Pseudomonas putida*. CYP101 has provided a paradigm for P450 structure and function studies (*3*). CYP101 catalyzes the regio- and stereospecific hydroxylation of camphor by dioxygen to 5-*exo*-hydroxycamphor. Two redox proteins, putidaredoxin reductase (PdR), a flavoprotein NADH reductase, and putidaredoxin (Pdx), a $Cys_4Fe_2S_2$ ferredoxin, provide the electrons necessary for camphor hydroxylation (*4*). Pdx serves as the proximal electron donor for CYP101 and sequentially transfers two electrons from PdR to CYP101 per turnover, the second electron transfer being rate-limiting under physiological conditions (*5*). In addition, Pdx is an effector for substrate turnover by CYP101, and the complex between CYP101 and Pdx is the catalytically competent species (*6*).

Elucidation of the mechanism of electron transfer and the origin of the effector activity of the *in vivo* reductant Pdx is essential for understanding the CYP101 reaction cycle. While the availability of structures for CYP101 (*3*, *7*−*9*) and Pdx (*10*−*14*) has provided insight into mechanistic questions, the details of electron transfer and the origins of effector activity have not yet been determined. A number of kinetic (*5*, *15*), mutational (*16*−*18*), and theoretical studies (*19*, *20*) have been conducted to gain insight into the specific interactions between Pdx and CYP101. NMR techniques have emerged as an effective method for gaining insight into molecular recognition (*21*) and have been applied extensively to the investigation of the CYP101·Pdx system (*22*−*24*). In particular, mapping of chemical shift perturbations upon complex formation using NMR spectroscopy provides a sensitive

† This work was supported in part by a grant from the U.S. Public Health Service (R01-GM44191 to T.C.P.).

* To whom correspondence should be addressed. E-mail: pochapsk@brandeis.edu. Phone: (781) 736-2559. Fax: (781) 736-2516.

‡ Department of Chemistry.

§ Department of Biochemistry.

[1] Abbreviations: Cmp, chloramphenicol; CYP101, cytochrome $P450_{cam}$; CYP−S−CO, carbon monoxide and camphor-bound reduced cytochrome $P450_{cam}$; GC−MS, gas chromatography−mass spectroscopy; IPTG, isopropyl β-D-thiogalactoside; Kan, kanamycin; LB, Luria-Bertani medium; NMR, nuclear magnetic resonance; HSQC, heteronuclear single-quantum correlation; M9, minimal growth medium; OD_{600}, optical density at 600 nm; PdR, putidaredoxin reductase; Pdx, putidaredoxin; Pdx^r, reduced putidaredoxin; TROSY, transverse relaxation optimized spectroscopy.

10.1021/bi052318f CCC: $33.50
Published on Web 03/01/2006

tool for identifying the residues that are perturbed by these interactions (*21*). Our group recently reported the application of multidimensional NMR to the characterization of the complex between the Fe(II)−carbonmonoxy−camphor−CYP101 complex (CYP−S−CO) and reduced Pdx (Pdx^r) (*22*). The CYP−S−CO complex provides a convenient diamagnetic model for the one-electron reduced complex of CYP101 with camphor and O_2, an obligate intermediate in the reaction pathway. We found that the binding of Pdx^r to CYP−S−CO perturbs not only residues in the proposed Pdx binding site on CYP101 but also residues in regions remote from the binding site that are involved in substrate access to and orientation within the CYP101 active site. These observations suggested to us that the primary role of the effector is to prevent the loss of substrate and/or intermediates from the active site and to ensure that the substrate is in the correct orientation for reaction by selecting the active (closed) conformation of CYP101 from a manifold of conformations occupied in the absence of effector.

If the Pdx-induced perturbations in the CYP101 structure are indeed critical for effector activity, other identified effectors of CYP101 should induce spectral perturbations similar to those observed in the presence of Pdx. In our previous study, we found that adrenodoxin, a ferredoxin structurally and functionally similar to Pdx that is not an effector of CYP101 turnover, did not induce any obvious spectral changes in CYP101 in molar excesses up to 5-fold. On the other hand, cytochrome b_5 has previously been reported to act as an effector for camphor hydroxylation by CYP101 (*6*) and is a good candidate for establishing which structural perturbations observed in the presence of Pdx are related to effector activity. Cytochrome b_5 is an integral membrane protein consisting of an amino-terminal hydrophilic domain that contains a single heme *b* with two histidines as axial ligands for the iron and a carboxyl-terminal membrane-binding region (*25*). The soluble heme-containing domain of cytochrome b_5 is small (11 kDa) and structurally well characterized. Cytochrome b_5 participates in electron transfer processes in a number of biological redox pathways and shows effector activity for some class II cytochrome P450s, including CYP3A4 and CYP2B4 (*25*, *26*). The reduction potentials of cytochrome b_5 and ferric CYP101 are approximately 25 and −300 mV, respectively, making cytochrome b_5 unable to donate the first electron to CYP101 (*25*). Sligar and colleagues showed that cytochrome b_5 is a competitive inhibitor of electron transfer from Pdx to CYP101 and proposed that cytochrome b_5 and Pdx bind to similar sites on the CYP101 surface (*27*). In this work, we show via multinuclear NMR methods that cytochrome b_5 perturbs many of the same resonances in CYP−S−CO as Pdx, including those for residues involved in substrate access to and orientation within the active site of CYP101. We also confirm that the particular construct of cytochrome b_5 used for these studies is an effector for CYP101 enzymatic activity. Finally, we discuss the common features of the two complexes in terms of their implications for the mechanism of effector activity.

MATERIALS AND METHODS

Protein Expression and Purification. Perdeuterated [U-^{15}N]-CYP101 was overexpressed, isolated, and purified from *Escherichia coli* strain NCM533 harboring the pDNC334A plasmid that encodes the C334A mutant of CYP101 under control of the *lac* promoter. The C334A mutant is identical to the wild-type monomer in terms of enzymatic activity and spectroscopic properties but does not dimerize even at millimolar concentrations (*28*). Cell growth was performed at 37 °C with shaking, which was started by inoculating a freshly transformed colony into 5 mL of LB supplemented with 25 μg/mL chloramphenicol (Cmp) and 50 μg/mL kanamycin (Kan). When the optical density at 600 nm (OD_{600}) reached 0.6, the starter culture was scaled up to 50 mL in LB medium, which was subsequently spun down at an OD of 0.6, resuspended in 50 mL of M9 medium, and incubated for 2 h. M9 medium (per liter) contains 6.8 g of Na_2HPO_4, 3 g of KH_2PO_4, 0.5 g of NaCl, 1 g of NH_4Cl, 2 mM $MgSO_4$, 0.04 mM $CaCl_2$, 0.01 mM $FeCl_3$, 0.5% glycerol, 0.25 mg of thiamine, 25 mg of Cmp, 50 mg of Kan, and 2 mL of a trace metal mix stock solution containing 34.36 g of H_3BO_3, 4.32 g of $MnCl_2 \cdot 4H_2O$, 0.315 g of $ZnCl_2$, 0.03 g of MoO_3, 0.003 g of $CuSO_4 \cdot 5H_2O$, and 0.012 g of $CoCl_2 \cdot 6H_2O$ per liter. The cell culture was then pelleted via centrifugation and resuspended in 1 L of fresh M9+ medium prepared using $^{15}NH_4Cl$, fully deuterated d_8-glycerol, and 99.9% D_2O (Cambridge Isotope Laboratories, Inc., Andover, MA). When the OD_{600} reached 1.0, 70 mg of porphyrin precursor δ-aminolevulinic acid (Sigma, St. Louis, MO) was added, followed by the addition of IPTG to a final concentration of 1 mM to induce protein expression. Finally, the culture was harvested after incubation for 12 h.

Purification of CYP101 followed published procedures (*29*) with modifications. Briefly, 10 g of cell paste resuspended in 40 mL of buffer L [50 mM Tris-HCl (pH 7.4), 50 mM KCl, and 1 mM camphor] was disrupted by sonication using a Misonix (Farmingdale, NY) sonicator 3000 eight times for 30 s spaced by 30 s rest intervals at a power setting of 55%. All sonications were performed with cooling in an ice bath. Following centrifugation at 32000*g* for 50 min to remove the cell debris, 200 mg of protamine sulfate (Sigma) dissolved in 5 mL of buffer L was added dropwise with stirring to the protein solution to precipitate DNA, which was then removed by centrifugation. The resulting supernatant was precipitated by addition of ammonium sulfate to a w/v of 70%. After solution of the pellet, dialysis, and concentration, the protein was applied to a DEAE-Sepharose fast flow anion-exchange column (Amersham Biosciences, Piscataway, NJ) and developed with a linear gradient from 50 to 300 mM KCl. Finally, the protein solution was subjected to size exclusion on a P-100 column (Bio-Rad) equilibrated and developed with buffer L. The fractions with an A_{391}/A_{280} value greater than 1.45 were pooled and used for the NMR experiments.

Perdeuterated cytochrome b_5 was purified from *E. coli* BL21(DE3) cells containing the pETb5 plasmid that encodes the gene for the 98-residue soluble core domain of rat cytochrome b_5 under the control of the T7 promoter (*30*). Growth and expression of cytochrome b_5 followed a procedure similar to that used for CYP101 with the exception that 0.3% d_6-glucose (Cambridge Isotope Laboratories) was used as the carbon source in the D_2O-based M9 medium. For purification, cell pellets were resuspended in 4 volumes of 50 mM Tris-HCl (pH 7.5) and 1.0 mM EDTA and lysed by sonication, followed by centrifugation to remove the cell debris. Cytochrome b_5 is isolated primarily as an apoprotein

from this overexpression system and was reconstituted with hemin (Sigma) prior to purification. Ten milligrams of hemin (iron protoporphyrin IX) was dissolved in a minimal volume of 0.1 N NaOH, diluted 10-fold with H_2O, and added dropwise to the lysate containing apocytochrome b_5 with stirring. Reconstitution was monitored by periodically removing aliquots for a spectroscopic assay and was terminated when the absorbance at 414 nm maximized and a shoulder began to appear on the same peak. Excess hemin was then precipitated by lowering the pH of the protein solution to 6.0 and removed by filtration though 0.45 μm filter paper. The clarified cytochrome b_5 holoprotein solution was loaded onto a Whatman DE-52 ion-exchange column and eluted with a linear 0 to 0.4 mM NaCl gradient at a flow rate of 1 mL/min. Fractions with an A_{413}/A_{280} value of >3.5 were pooled and concentrated using Amicon centrifugal concentrators (Millipore, Bedford, MA) and applied to a Biogel P-30 (Bio-Rad) size exclusion column. Fractions with an A_{413}/A_{280} value of >5.7 were pooled, concentrated, and used for NMR experiments. Protein concentrations and absorbance ratios for both enzymes were estimated by UV−visible spectroscopy using available extinction coefficients (*29*, *30*). Conditions for preparation and purification of isotopically labeled Pdx have been described previously (*22*).

NMR Sample Preparation. Concentrated protein samples were exchanged either into 10% D_2O/90% H_2O NMR buffer [50 mM Tris-d_{11}-HCl (pH 7.4), 100 mM KCl, and 2 mM *d*-camphor] for $^1H-^{15}N$ HSQC experiments or into 100% D_2O NMR buffer for one-dimensional NMR experiments using spin columns packed with P-2 resin (Bio-Rad). Reduction of CYP101 (0.5 mM), Pdx (3 mM), and cytochrome b_5 (9 mM) was achieved by addition of aliquots of 0.25 and 1 M sodium dithionite [prepared in degassed 1 M Tris-HCl (pH 8.0)] with a slight excess of reductant compared to the amount of protein. All protein samples were placed under a CO atmosphere prior to and after the addition of the reducing agent for 10 and 2 min, respectively. CYP−S−CO samples thus obtained were then transferred to an NMR sample tube (Shigemi, Inc., Allison Park, PA) inside an anaerobic chamber under a N_2 (90%)/H_2 (10%) atmosphere, and the NMR tube was sealed with Parafilm (Pechiney Inc., Menasha, WI) before being removed from the anaerobic chamber. Aliquot additions of the desired protein (cytochrome b_5 or Pdx^r) to the deuterated ^{15}N-labeled CYP101 samples for NMR titrations were performed in the anaerobic chamber. For titrations with cytochrome b_5, the molar ratio between the two proteins was varied from 0 to 16, in six titration points. The Pdx^r titration was performed as described previously (*22*).

NMR Experiments. NMR titrations of CYP−S−CO with cytochrome b_5 were performed at 298 K on a 14 T Varian UNITY Inova spectrometer operating at 599.702 and 60.774 MHz for ^1H and ^{15}N, respectively. The spectrometer is equipped with a pulsed field gradient amplifier and a 5 mm $^1H\{^{13}C,^{15}N\}$ triple-resonance PFG probe. $^{15}N-^1H$ TROSY-HSQC spectra (*31*) were acquired to follow the chemical shift perturbations of NH-coupled pairs during titrations. For these experiments, gradient coherence selection was used to select desired coherences and suppress solvent signals, and the Rance−Kay method was used to obtain quadrature detection in the indirectly detected dimension (*32*, *33*). Spectra were acquired with 596 (^1H) × 128 (^{15}N) complex points, a ^1H sweep width of 8000 Hz, and a ^{15}N sweep width of 2200 Hz. All ^1H and ^{15}N chemical shifts (δ) are reported in parts per million relative to trimethylsilylpropionic acid sodium salt. All of the NMR spectra were processed and analyzed using the Topspin software package (Bruker Biospin). Conditions for the titration of CYP−S−CO with Pdx^r were described previously (*22*).

Estimation of K_d for the Cytochrome b_5−CYP−S−CO Complex. For 18 ^{15}NH pairs with well-resolved resonances for each titration point, ^1H chemical shifts (δ) measured in hertz were fit to the following standard equation using the nonlinear regression analysis package of Mathematica 5.2:

$$\delta = \delta_0 + (\delta_{max} - \delta_0)\{K_d + m_0 + p_0 - [(K_d + m_0 + p_0)^2 - 4m_0p_0]^{1/2}\}/2m_0 \quad (1)$$

where δ_0 and δ_{max} are the chemical shifts of the free and bound forms of CYP101, respectively, and m_0 and p_0 are the nominal concentrations of CYP101 and cytochrome b_5, respectively. The fits yielded values for δ_{max} and K_d.

Enzymatic Substrate Turnover with Cytochrome b_5 as the Effector. The turnover of camphor yielding 5-*exo*-hydroxycamphor by CYP101 with cytochrome b_5 as the effector was monitored using gas chromatography−mass spectrometry (GC−MS) (*6*). CYP101 in 50 mM potassium phosphate buffer (pH 7.4) was added anaerobically to a solution containing 1 mM camphor, 4 μM proflavine, and 10 mM EDTA to a final concentration of 4 μM. The CYP101 was then photoreduced by exposure to a 400 W white light source. The mixture was then oxygenated by injection of air, and cytochrome b_5 was injected to a final concentration of 64 μM to initiate the hydroxylation reaction. After 1 h, the mixture was extracted with dichloromethane and analyzed with a Hewlett-Packard 5890 GC−MS spectrometer equipped with an HP-5MS column (30 m × 0.25 mm × 0.25 μm, Agilent Technologies, Inc., Palo Alto, CA), a quadrupole mass spectrometer, and a flame ion detector. The injector and flame ionization detector were maintained at 220 and 230 °C, respectively, and a split ratio of 3:1 was used. The He carrier flow rate was kept at 1.0 mL/min. The temperature program was as follows: 60 °C for 3 min and from 60 to 210 °C at a rate of 5 °C/min. Under these conditions, camphor (*m*/*z* 152) elutes at 9.0 min and hydroxycamphor (*m*/*z* 168) elutes at 12.3 min. Pdx added to a similar reaction mixture provided a positive control, and the photoreduced CYP101 solution without effector added provided the negative control.

RESULTS

Chemical Shift Perturbations in the Pdx^r−CYP−S−CO Complex. We have previously described the use of two-dimensional $^1H-^{15}N$ TROSY-HSQC NMR experiments to monitor the titration of perdeuterated [U-^{15}N]CYP−S−CO with Pdx^r (*22*). As a significant number of backbone resonances have been additionally assigned in the CYP−S−CO spectrum since our last report (*22*), the results of those titrations can now be more completely analyzed. Furthermore, some ambiguities concerning perturbations in crowded regions of the spectrum have been resolved, and a number of resonances that we previously reported as unperturbed are now seen to be perturbed upon addition of Pdx^r. Among the newly assigned resonances, perturbations are observed

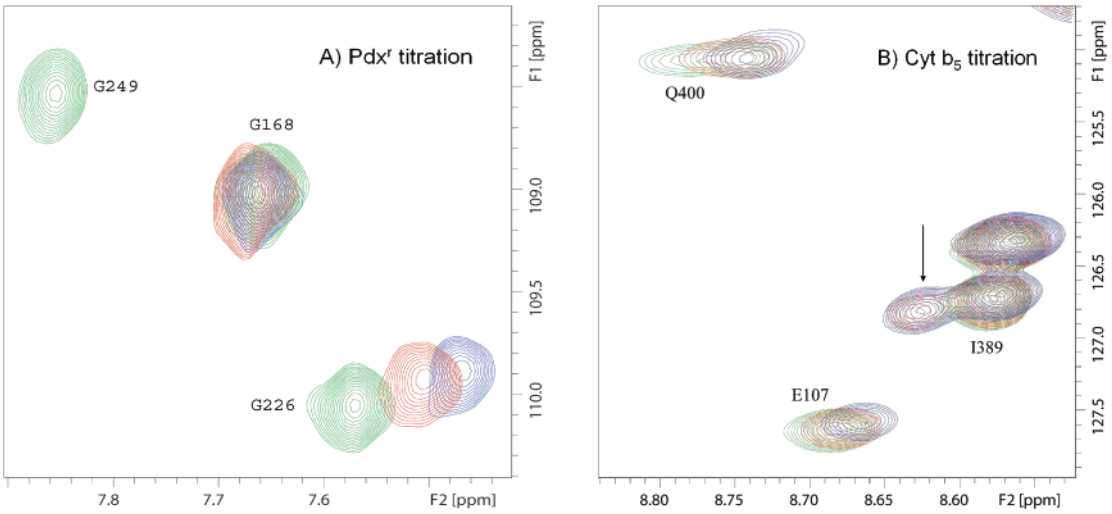

FIGURE 1: Superimposed 14 T (600 MHz ^{1}H) ^{1}H−^{15}N TROSY-HSQC spectra showing different types of titration effects in CYP−S−CO with Pdx^r or reduced cytochrome b_5. Color coding of peaks is as follows: green for no Pdx or cytochrome b_5, red for ~0.5 equiv of Pdx or 4 equiv of cytochrome b_5, and blue for 1 equiv of Pdx or 16 equiv of cytochrome b_5. (A) Portions of the superposition of the amide region of the ^{1}H−^{15}N TROSY-HSQC spectra (600 MHz ^{1}H, 17 °C, 10% D_2O/90% H_2O, 50 mM Tris-d_{11}-HCl, pH 7.4, 100 mM KCl, and 2 mM *d*-camphor) as a function of the concentration of added Pdx^r. Gly 226 is shifted upon addition of Pdx; Gly 168 is unperturbed by Pdx, while Gly 249 is broadened to invisibility at the first addition of Pdx. (B) Portions of the superposition of the amide region of the ^{1}H−^{15}N TROSY-HSQC spectra (600 MHz ^{1}H, 25 °C, 10% D_2O/90% H_2O, 50 mM Tris-d_{11}-HCl, pH 7.4, 100 mM KCl, and 2 mM *d*-camphor) as a function of the concentration of added cytochrome b_5. Glu 107 and Gln 400 are shifted upon addition of cytochrome b_5, while Ile 389 shows peak splittings (indicated with an arrow) that increase in intensity with an increase in cytochrome b_5 concentration.

at the backbone NH resonances of Arg 109, Phe 111, Ala 115, and Val 118 in the N-terminal and middle regions of the C helix (residues 106−126), Ser 190 in the F−G loop, Thr 192 and Phe 193 in the N-terminal end of the G helix (residues 192−214), Thr 252 in the center of the I helix (residues 234−267), and residues His 347, Phe 350, Gly 351, Gly 353, Ser 354, Leu 358, and Gly 359 within the Cys ligand loop (residues 350−357). The NH resonance of the axial heme ligand, Cys 357, has not yet been identified; however, the NH resonance of Leu 358 is shifted upfield by 2.75 ppm due to the shielding effect of the heme, an unusually large shift, and it is possible that the Cys 357 NH proton resonates near or under the water peak at 4.78 ppm. Residues previously classified as ambiguous or unperturbed by Pdx addition that are now classified as perturbed include Gly 37, Ser 48, Val 50, and Asp 52 in the A helix and A−β1 loop, Ala 92 in the B′ helix, Gln 108 in the C helix, Gly 168 and Glu 173 in the E−F loop, Ala 196 and Ile 208 in the G helix, and Val 338, Ile 388, and Gln 289 in the β5 sheet. All of these observations support our previous identification of the CYP101 structural features perturbed by binding of Pdx (*22*). In particular, the first three turns of the C helix (residues 107−118), previously proposed as a primary interaction site for Pdx (*19*), are now seen, along with the preceding B′ helix, to be among the CYP101 structural features most uniformly affected by Pdx binding.

Previously, we classified the CYP−S−CO resonances perturbed by Pdx^r binding as being either in the slow/intermediate-exchange regime or in the fast-exchange regime (*22*). A nonlinear fit of chemical shift as a function of Pdx concentration to eq 1 for resonances in the fast-exchange regime yields a K_d value of 26 ± 12 μM for the Pdx^r−CYP−S−CO complex (ref *22* and Figure 1A). The apparent exchange rate of the complex at half-saturation was estimated from line width measurements for resonances in the fast-exchange regime to be ~300 s^{-1} at 17 °C (*22*, *34*). As expected, all resonances in the fast-exchange regime show ^{1}H shift perturbations with a $\Delta\delta_{max}$ of <300 s^{-1}, as determined from the value for $\Delta\delta_{max} = \delta_o - \delta_{max}$ obtained from fits of experimental shifts to eq 1.

Resonances identified as being in the slow/intermediate-exchange regime are broadened to invisibility upon the first addition of Pdx^r (CYP101:Pdx molar ratio of 5:1) and are for the most part observed for residues in the proximity of the heme and/or active site, including the heme axial ligand loop containing Cys 357 and portions of the C and I helices (see Figure 5C). On the basis of their disappearance in the first titration point, they are assumed to have chemical shift differences ($\Delta\delta$) between the Pdx-bound and free forms of >300 s^{-1} at 17 °C, although the chemical shifts of these resonances in the bound form have not confirmed. Recently, we detected a high-barrier conformational shift in the active site of CYP101 that occurs upon Pdx binding, and by comparing chemical shift changes for the 8-CH_3 (which is in slow exchange) and 9-CH_3 (which is in fast exchange) of bound camphor (*34*), we estimated an exchange rate over this barrier between 150 and 300 s^{-1} at 25 °C. On the basis of the similarities of the rates obtained from two different observations [line widths (*22*) and camphor ^{1}H shifts (*34*)] as well as the proximity of NH resonances undergoing slow/intermediate exchange to the active site, we find it likely that the same event is responsible for both observations. The precise nature of this high-barrier event is currently under investigation in our laboratory.

In addition to these two categories of perturbations, some resonances, most prominently around the region of the A−β1 loop (residues 47−51) and β1 strand (residues 52−66), are observed to split into two peaks during the titration and the intensities of the new peaks increase with the increasing Pdx^r concentration. Although this splitting represents a slow-exchange event, the lack of any significant line broadening associated with the splitting, as well as the small chemical

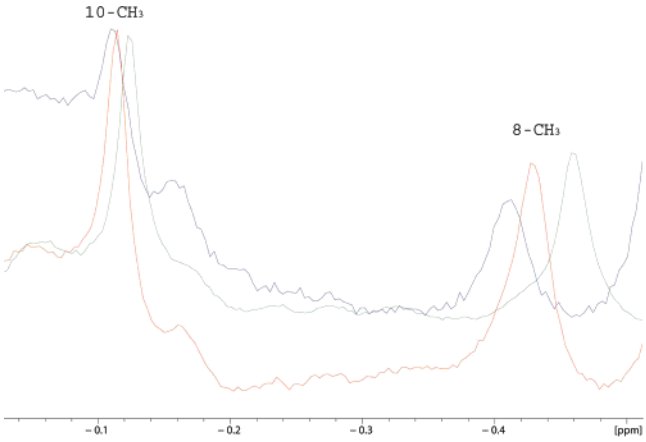

FIGURE 2: Superposition of the upfield region of 600 MHz ^{1}H NMR spectra showing titration of perdeuterated CYP−S−CO with perdeuterated cytochrome b_5 in 100% D_2O, 50 mM potassium phosphate buffer (pH 7.4), and 50 mM KCl. The 8-CH_3 group of camphor shifts downfield upon titration of cytochrome b_5, while the 10-CH_3 group moves very slightly [$\Delta\delta_{max(obs)} < 10$ Hz] but noticeably downfield. The camphor 9-methyl resonance is not appreciably perturbed (peak not shown). One division on the chemical shift axis = 0.02 ppm = 12 Hz. Color coding of spectra follows the convention of Figure 1.

shift differences between the split peaks (less than 50 Hz, in some cases), indicates that the exchange that is involved is considerably slower than that associated with the high-barrier event discussed above and is likely not related to the conformational changes responsible for the slow/intermediate-exchange perturbations discussed in the preceding paragraph. As such, it appears that there is more than one slow conformational change induced by Pdx in the CYP101 structure, one that affects the active site, substrate, and adjacent structural features [the "high-barrier event" (*34*)], and another, slower event that connects conformations in regions remote from the active site in the A−β1 loop and β1 strand.

Chemical Shift Perturbations in CYP−S−CO Due to Cytochrome b_5. Two-dimensional ^{1}H−^{15}N TROSY-HSQC NMR experiments were used to monitor the titration of perdeuterated [U-^{15}N]CYP101 with unlabeled cytochrome b_5. Chemical shift perturbations were observed in the spectrum of CYP−S−CO upon binding of cytochrome b_5 (Figure 1B). Unlike the case for Pdx, we did not observe the disappearance or significant exchange broadening of any amide ^{1}H resonance in the CYP−S−CO complex due to the addition of cytochrome b_5, although a slight exchange broadening is observed at high resolution to the camphor 8-methyl peak (Figure 2). Instead, chemical shifts change in a continuous fashion during the titration; that is, a single resonance peak is observed for each perturbed resonance of CYP−S−CO at any point during the titration. These results indicate that the CYP−S−CO·cytochrome b_5 complex is in fast exchange on the ^{1}H chemical shift time scale between bound and unbound forms. In general, the chemical shift changes observed in CYP−S−CO upon complexation with cytochrome b_5 are smaller in magnitude than those induced by Pdx^r binding (Figure 3). However, the perturbations can be interpreted with confidence, and only peaks with a $\Delta\delta_{max(obs)} > 10$ Hz are considered as being perturbed by addition of cytochrome b_5. Nonlinear fits of chemical shift changes for 18 affected resonances to eq 1 as a function of cytochrome b_5 and CYP−S−CO concentrations yield a K_d of 13 ± 3 mM in 50 mM Tris-HCl buffer at pH 7.4 and 25 °C with 100 mM KCl and 2 mM camphor. The uncertainty represents the reproducibility of fitting the ^{1}H chemical shift induced by titration with cytochrome b_5 for 18 residues in CYP−S−CO.

As was the case with Pdx, we observe that some NH resonances of CYP101 split in the presence of cytochrome b_5, indicating that a minor conformation is populated under these conditions at slow exchange with the major ensemble. Splittings are observed primarily in the A−β1 loop, the N-terminus of strand β1, and the C and G helices, with scattered resonances splitting in the A helix, B helix, E helix, and β2 sheet. As was the case with Pdx, the structural origins of this phenomenon are unknown; however, it is apparently not related to the high-barrier conformational shift that occurs when Pdx binds to CYP101 (see ref *34*), and no phenomenon corresponding to that high-barrier event is observed in the course of the cytochrome b_5 titration.

Perturbations induced in CYP101 by cytochrome b_5 binding were mapped, and the distribution of the perturba-

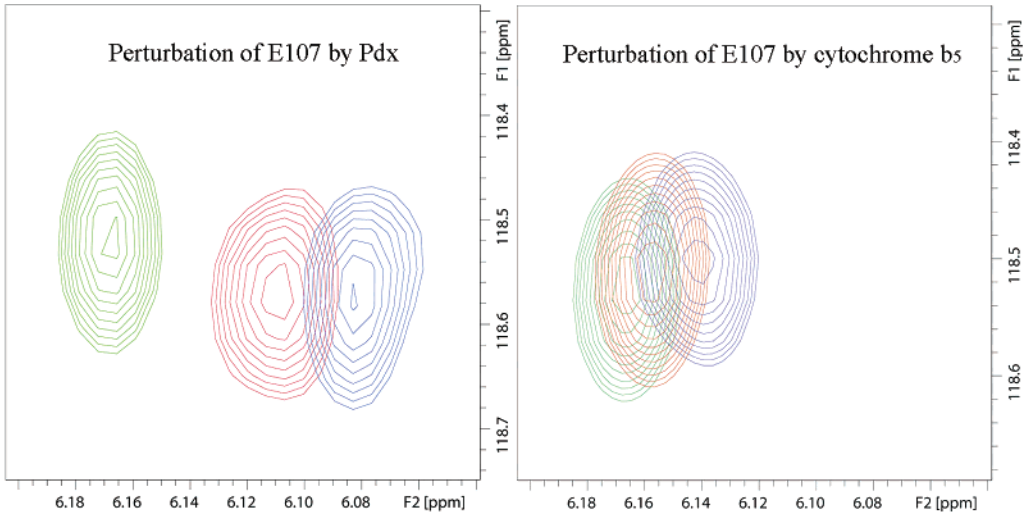

FIGURE 3: Comparison of the magnitudes of the chemical shift changes for the NH correlation of the same residue (Glu 107 in the C helix) of CYP101 upon complexation with Pdx^r and cytochrome b_5 in superimposed 14 T (600 MHz ^{1}H) ^{1}H−^{15}N TROSY-HSQC spectra. The color coding of the peaks follows the convention in Figure 1.

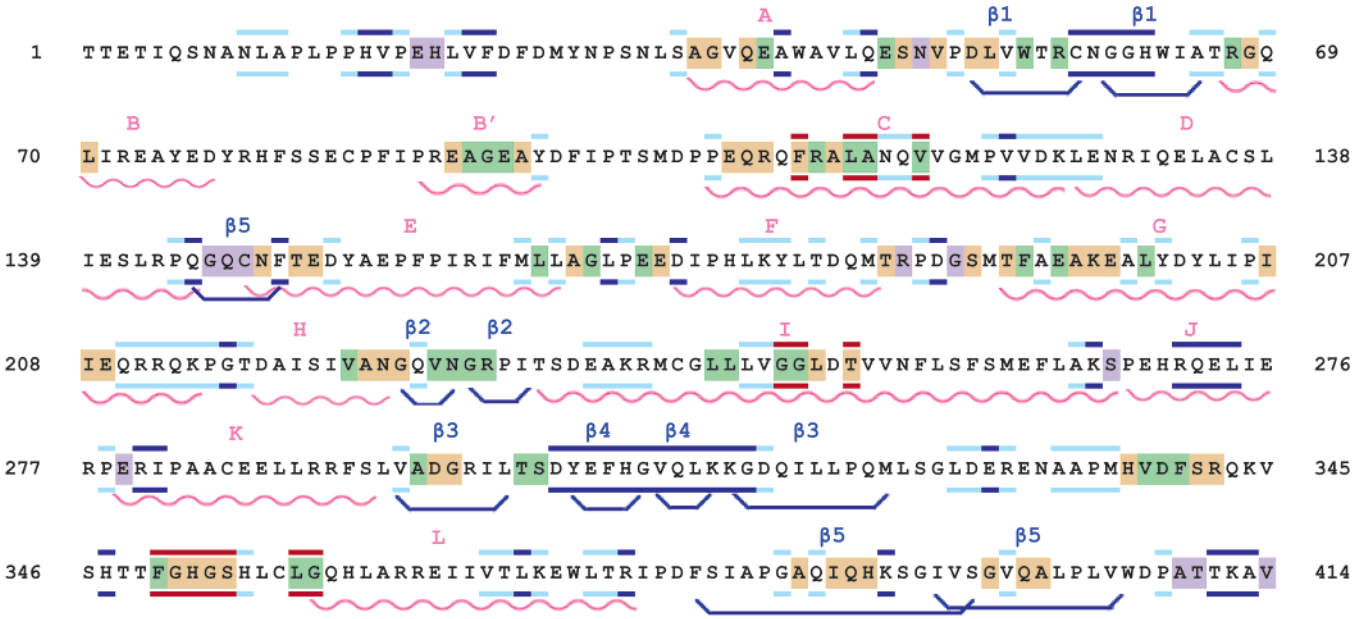

FIGURE 4: Amino acid sequence of CYP101, color-coded to show the structural perturbations due to Pdx^r and cytochrome b_5 mapped via $^1H-^{15}N$ HSQC experiments. Wavy red lines indicate helices, and boat-shaped lines in black indicate β-sheets. Secondary structural features are named above the sequence using the nomenclature of Raag and Poulos (*8*). Residues whose amide NH groups are perturbed in CYP−S−CO upon addition of either cytochrome b_5 or Pdx^r are highlighted in beige, in green if perturbed by only Pdx^r, and in purple if perturbed by only cytochrome b_5. Residues bordered in red are broadened to invisibility or shifted to unknown positions upon the first addition of Pdx^r; those bordered in dark blue denote resonances that are unperturbed by addition of either Pdx^r or cytochrome b_5, and those bordered in light blue are residues whose NH correlations have been assigned but for which perturbations due to effector addition are ambiguous due to spectral overlap.

tions related to both the sequence and the three-dimensional structure of CYP−S−CO (Figures 4 and 5A). As can be seen from these figures, binding of cytochrome b_5 perturbs many of the same regions that Pdx binding does (*22*), including the C helix, portions of the F helix, the F−G loop, and the G helix as well as portions of the Cys 357 loop. Other regions perturbed by both Pdx and cytochrome b_5 include both ends of the E helix and portions of sheets β3 and β5. A number of regions are affected by only cytochrome b_5 and not by Pdx, including several residues in the F−G loop (Arg 187 and Gly 190), one strand of the β5 sheet (Gly 146−Asn 149), and residues near the C-terminus of CYP101, Ala 409, Thr 410, and Val 414.

Perturbation of Bound Camphor by Cytochrome b_5. We titrated samples of perdeuterated CYP−CO−S in D_2O with perdeuterated cytochrome b_5 to observe any effects that the addition of cytochrome b_5 might have on the orientation of camphor bound in the active site. Unlike Pdx, reduced cytochrome b_5 has a large number of resonances in the same region of the ^1H NMR spectrum as the methyl groups of bound camphor. Although perdeuteration of cytochrome b_5 significantly reduces the interference of the cytochrome b_5 signals with the camphor methyl ^1H signals, at higher ratios of cytochrome b_5 to CYP−S−CO, residual protonation of cytochrome b_5 results in some complexity in this region of the spectrum. Still, the three methyl signals of CYP101-bound camphor, 10-CH_3, 8-CH_3, and 9-CH_3, in the upfield region of the ^1H spectrum of perdeuterated CYP−S−CO can be observed in the absence and presence of perdeuterated cytochrome b_5 and on the basis of the assignments reported recently by our group (*34*) can be followed with confidence during the titration. Of the three camphor methyl signals, the 9-CH_3 resonance did not show significant perturbation, the 10-CH_3 ^1H resonance showed some minimal titratable movement with a $\Delta\delta_{max(obs)}$ of <10 Hz, and the 8-CH_3 ^1H resonance is perturbed slightly ($\Delta\delta_{max}$ = 30 Hz) by the addition of cytochrome b_5 (Figure 2). The ^1H resonance of 8-CH_3 moves in a continuous fashion during the titration with only minimal line broadening, again indicating that a fast-exchange event is being monitored.

Confirmation of Cytochrome b_5 Effector Activity. The original reports concerning the effector activity of cytochrome b_5 in the reconstituted CYP101 turnover assay were made using a trypsin-solubilized form of cytochrome b_5 obtained from liver homogenates (*6*). As a bacterially expressed cytochrome b_5 construct was used in our experiments, we needed to confirm that this construct also exhibits effector activity in the reconstituted CYP101 system. We used GC−MS to detect CYP101 substrate turnover in the presence of cytochrome b_5 and have confirmed that the current construct used in the NMR studies is capable of supporting turnover under the conditions reported by Lipscomb and Gunsalus (*6*). Addition of either cytochrome b_5 or Pdx to photoreduced and oxygenated camphor-bound CYP101 resulted in the formation of 5-hydroxycamphor (Figure 6) under the reported conditions (*6*), while in the absence of effector, hydroxycamphor formation was not detected. The experiment was carried out in triplicate, and the results were consistent.

DISCUSSION

A Model for Cytochrome b_5−CYP101 Interactions. As was previously observed with Pdx, the titration of CYP−S−CO with cytochrome b_5 affects structural features throughout the CYP101 molecule. However, the perturbations observed with cytochrome b_5 are generally smaller than the corresponding perturbations in the Pdx^r−CYP−S−CO complex. The cal-

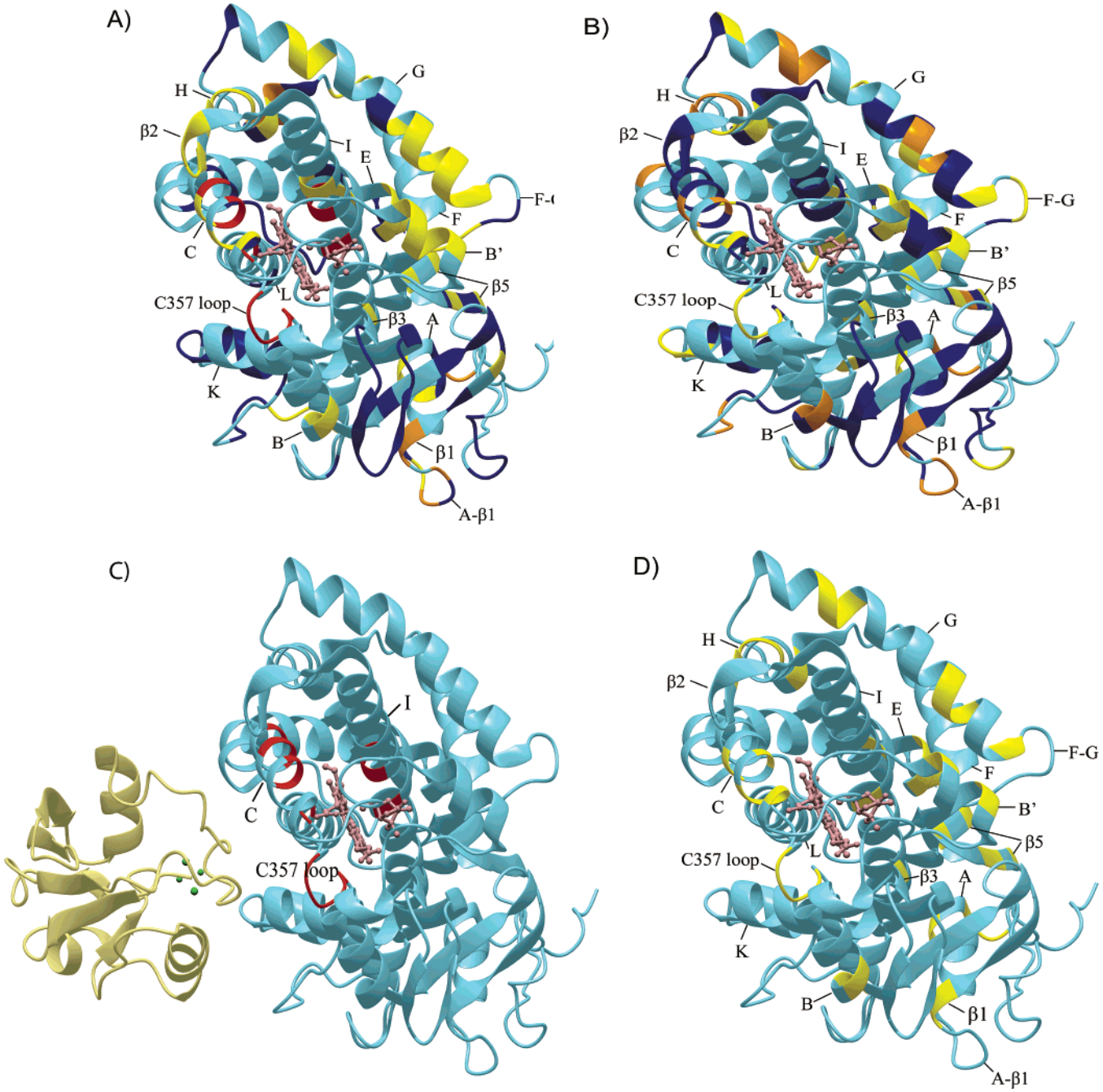

FIGURE 5: CYP101 structure (PDB entry 3CPP) color-coded to show the distribution of secondary structural features perturbed by Pdx or cytochrome b_5 as determined by NMR. Structural features colored dark blue are not affected by either Pdx or cytochrome b_5 binding; they are colored yellow if they are perturbed ($\Delta\delta_{max} < k_{ex}$), orange if peak splitting occurs, and red for resonances that are essentially undetectable after the first addition of Pdx ($\Delta\delta_{max} \sim k_{ex}$). Features for which insufficient data are available are colored light blue. The heme and camphor are colored pink. (A) Perturbation caused by Pdx^r, updated from Figure 4 of ref *22* to include newly assigned residues. (B) Perturbations caused by cytochrome b_5. (C) Only resonances that are essentially invisible after $^1/_5$ equiv of Pdx^r (colored beige) are localized on the CYP101 structure and colored red. The complex shown is that proposed in ref *19*. (D) Interior and partially solvent-exposed residues in the CYP101 structure affected by both Pdx and cytochrome b_5 titration. Perturbed residues are colored yellow. This figure was generated using MolMol (*40*).

culated dissociation constant for the CYP−S−CO complex with cytochrome b_5 (13 ± 3 mM at 25 °C) is 3 orders of magnitude higher than that of the CYP−S−CO−Pdx^r complex calculated previously at 17 °C, 26 ± 12 μM (*22*) (Figure 7). As it takes <3 equiv of Pdx to saturate CYP101 in the complex, the experimental $\Delta\delta_{max(obs)}$ values obtained from the last reported titration point with Pdx (2:1 Pdx:CYP101 ratio) are close to the $\Delta\delta_{max}$ values calculated from nonlinear fits to eq 1 (*22*). It would require approximately 30 equiv of cytochrome b_5 to saturate CYP−S−CO based on the calculated K_d for that complex. However, such a large excess of cytochrome b_5 is not practical in multidimensional NMR experiments. Consequently, we chose 16 equiv of cytochrome b_5 as the final titration point, and under these conditions, observed chemical shift perturbations are not maximal.

Sligar and Stayton demonstrated that the same cytochrome b_5 construct used in our study is a competitive inhibitor of

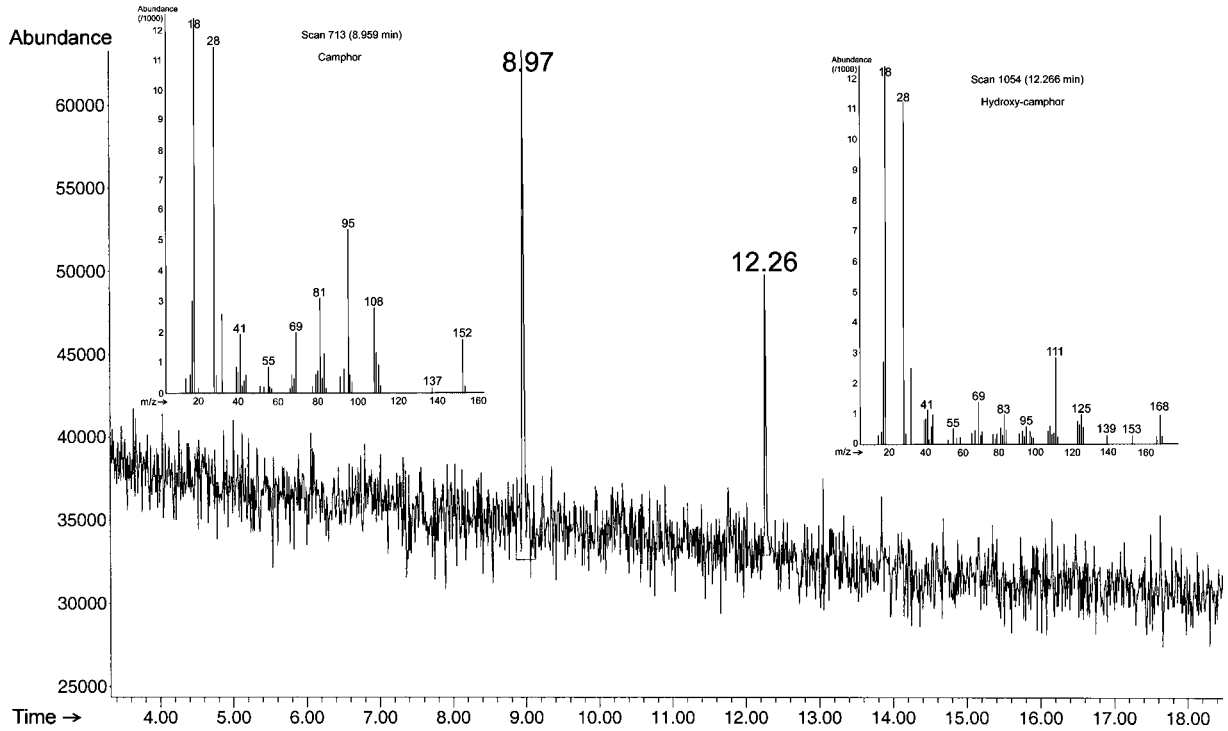

FIGURE 6: Elution profile of substrate turnover by CYP101 using cytochrome b_5 as an effector monitored by GC−MS. MS data for the substrate (camphor, eluted at 8.97 min with an ion at *m*/*z* 152) and product (5-hydroxycamphor, eluted at 12.26 min with an ion at *m*/*z* 168) are shown in the insets. Reaction conditions are detailed in Materials and Methods.

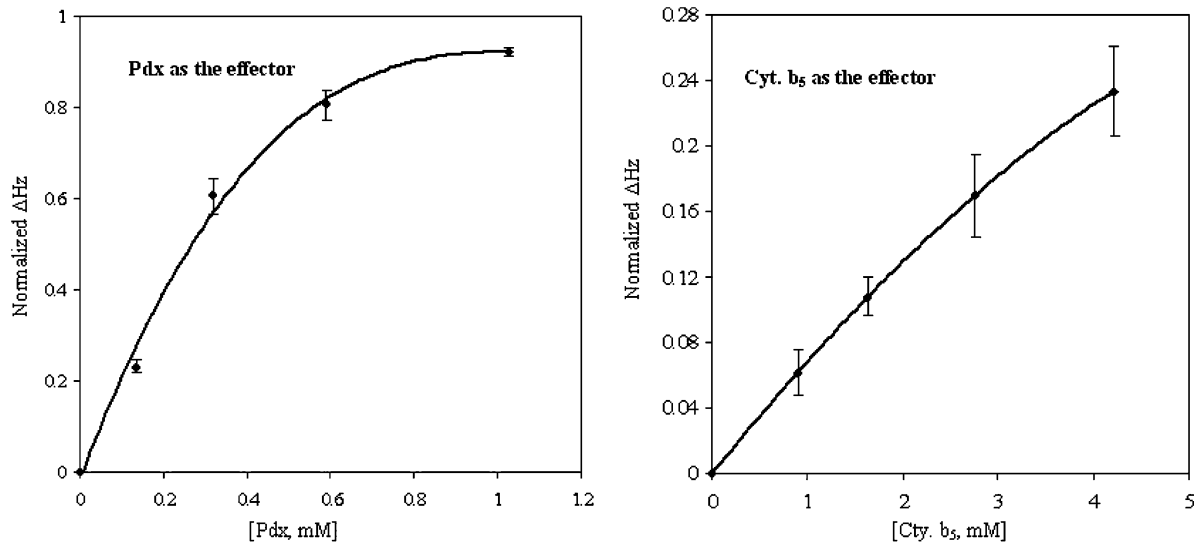

FIGURE 7: Normalized chemical shift perturbations of amide proton resonances in CYP101 as a function of titrant concentration (Pdx^r or cytochrome b_5). Vertical axis values are $\Delta\delta$ values at each titration point normalized to $\delta_{max} - \delta_0$, where δ_{max} was calculated by fitting titration data to eq 1 using the nonlinear regression analysis package of Mathematica 5.2. Chemical shifts of five residues in CYP101 monitored throughout the Pdx^r titration and 10 residues monitored throughout the cytochrome b_5 titration were fit to the binding curves. The curves represent the expected normalized chemical shift value given the calculated K_d and starting CYP101 concentration (see Materials and Methods for further details). For a CYP−S−CO starting concentration of 0.5 mM in both cases, the Pdx^r titration shows almost complete saturation at 1 mM Pdx, while the curve for the cytochrome b_5 titration is still nearly linear at much higher cytochrome b_5 concentrations. Error bars represent the maximum deviation of the experimental chemical shift values for the resonances used in the analysis. The larger error for cytochrome b_5 vs Pdx titration points is due to the increased uncertainty of the value of δ_{max} obtained from the fit of the cytochrome b_5 data to eq 1.

binding of Pdx to CYP101 and proposed that portions of the Pdx binding site and cytochrome b_5 binding site(s) overlap on the surface of CYP101 (*27*). Specifically, they implicated Arg 72 (B helix), Arg 112 (C helix), Lys 344, and Arg 364 (in the L helix following the loop containing the heme axial ligand Cys 357) as possibly interacting with cytochrome b_5 on the proximal surface of CYP101. On the basis of the perturbations we observe, it is likely that cytochrome b_5 interacts with CYP101 directly at the C helix and the Cys ligand loop. Also, residues near Arg 72 in the B helix and near Lys 344 are perturbed, although neither of those residues has yet been assigned. However, none of the assigned resonances in the L helix are perturbed by cytochrome b_5, suggesting that Arg 364 is not involved in the

interaction. Furthermore, the possibility of direct interaction between cytochrome b_5 and CYP101 away from the proximal surface is suggested by doubling of resonances corresponding to residues in the G helix and residues in the A−β1 loop and β1 sheet in the presence of cytochrome b_5.

Comparison of Complexes of Cytochrome b_5 and Pdx with CYP101. Comparison of perturbation patterns in the CYP101 structure induced by cytochrome b_5 and Pdx suggests similarities between the two complexes. Although the extent and precise patterns of affected residues differ, most regions of the CYP101 structure that are affected by Pdx binding are perturbed to some extent by cytochrome b_5 as well (Figure 4). The secondary structural features that are most uniformly perturbed by both cytochrome b_5 and Pdx include the N-terminal regions of the A (residues 36−39) and C helices (residues 107−113), the A−β1 loop (residues 48−52), and the loop containing the heme axial ligand cysteine (residues 351−354). Other regions that are perturbed in both complexes include the N-terminus of the B helix and portions of the B′, G, and I helices. The B′ helix is uniformly perturbed by Pdx^r, although only two residues, Glu 91 and Ala 95, are noticeably perturbed by cytochrome b_5.

In many cases, the differential perturbation patterns due to Pdx and cytochrome b_5 within affected secondary structural features may simply be a reflection of the weaker interaction of cytochrome b_5 with CYP101 than with Pdx, and perturbations that are apparent with Pdx are too small to be detected in the absence of a saturating concentration of cytochrome b_5. Nevertheless, as seen in the comparison in Figure 5, there are differences between the complexes besides the differences in binding affinity. Parts of the of β2 sheet (residues 226−233) are perturbed by Pdx association, but not by cytochrome b_5; in contrast, binding of cytochrome b_5 perturbs the β5 strand (residues 146−150) preceding the E helix as well as some C-terminal and N-terminal residues that are not affected by Pdx^r. Taken together, these observations suggest that the binding sites on CYP101 for Pdx and cytochrome b_5 are not identical but overlapping and that cytochrome b_5 is less specific in its interactions with CYP101 than is Pdx.

The most obvious difference between the two complexes is the apparent absence in the cytochrome b_5 complex of the high-barrier conformational change observed upon binding of Pdx^r to CYP−S−CO. This conformational change results in a reorientation of the camphor molecule within the active site of CYP101 and is detected as a broadening to essential invisibility of many backbone amide resonances for residues adjacent to the heme and camphor binding site (vide supra and ref *34*). As a result of this conformational shift, most identified residues in the central I helix are heavily perturbed by Pdx binding, especially the central part of the helix containing residues bracketing the heme and active site. The event likely involves reorganization of side chains in the active site and may be responsible for the large chemical shift changes that occur for many functionally important residues (Leu 244, Leu 245, Leu 246, Gly 248, Gly 249, Leu 358, and Gly 359) upon binding of Pdx^r. Figure 6 shows the localization of the residues that are affected by the high-barrier event as reflected by the fact that they are undergoing perturbations that are slow on the ^{1}H chemical shift time scale upon binding of Pdx. The change is profound and appears to be forced with almost 100% efficiency by the binding of Pdx^r (that is, the equilibrium constant for the conformational change lies far to the right when Pdx is bound). However, when cytochrome b_5 binds (Figure 5B), perturbations to the I helix are much smaller in magnitude and only Leu 250 and Thr 252 are appreciably perturbed among the eight assigned residues in this region (Figures 4 and 5). Likewise, although both the C helix and Cys 357 heme ligand loop are affected by cytochrome b_5, evidence for the high-barrier conformational change is absent. The camphor 8-CH_3 resonance is perturbed upon cytochrome b_5 binding (Figure 2), and the shift is in the same downfield direction as that observed upon titration with Pdx (*34*). However, the magnitude of the effect is much smaller and fast on the chemical shift time scale in the case of the cytochrome b_5−CYP−S−CO complex.

Implications for Effector Activity. It was demonstrated some years ago that trypsin-solubilized bovine cytochrome b_5 is an effector for camphor hydroxylation by CYP101, albeit at much higher concentrations for full activity than the physiological effector and reductant Pdx. The effector concentrations necessary for the maximum yield of 5-*exo*-hydroxycamphor from photoreduced camphor-bound O_2−CYP101 were 0.16 and 2.6 μM for Pdx and cytochrome b_5, respectively (*6*). The work presented here indicates that, like binding of Pdx, that of cytochrome b_5 perturbs many of the regions involved in substrate access and orientation (*1*, *7*, *8*) and supports our previous suggestion that the primary role of the effector is to select the catalytically active conformation from an ensemble of conformations that are occupied in solution by the CYP101 molecule. In this conformation, active site access from solution is blocked, preventing the loss of substrate and/or intermediate, and the substrate orientation is appropriate for the observed chemistry. Note that this model does not preclude the possibility that effector binding may also make the rate-limiting second electron transfer more favorable, but currently, direct evidence for this is lacking.

For insight into the conformational changes involved in effector activity, one can look at perturbations that occur upon binding of an effector to CYP101 structural features with minimum surface exposure. Structural perturbations mapped by NMR may be caused by direct contact with a bound molecule or indirectly via conformational changes induced by the binding event (*34*). Figure 5D shows perturbations that occur due to binding of both effectors at residues that are partially or completely buried in the CYP101 structure. "Hot spots" for such changes are contact points between secondary structural features. The region of contact for helices G−I is one such place, as are points of contact for helices F, G, and B′, the F−G loop, and the β5 sheet. Again, many of these structural features have been implicated in substrate access and orientation (*7*, *35*, *36*). In a recent crystallographic study, it was found that binding of a modified camphor linked to an external ruthenium sensitizer to CYP101 exhibits a more open substrate access channel that involves displacements in the distal B′, F, and G helices as well as conformational changes in the I helix relative to the positions of these features in closed-channel CYP101 structures (*37*). It was suggested by the authors of this work that the F and G helices translate relative to the protein core to open the access channel and cause the N-terminus of the I helix to rotate to conserve interhelical contacts. On the basis

of the localization of internal changes to contact points between secondary structures detected in this work, it is likely that internal effects on the CYP101 structure detected by NMR upon binding of the effector are transmitted in a similar fashion.

It is worth considering how the internal perturbations discussed above might be transmitted from the effector binding site(s) on the proximal face of the protein (to the left in Figure 7) to the affected structural features on the distal side (the F, G, and B′ helices, the F−G loop, and sheet β5). It has been proposed that Pdx binds at the proximal surface of CYP101 and that electrostatic interactions involving Arg 109 and Arg 112 on the C helix contribute to the specificity of the association between these physiological redox partners (*18*, *19*). It has also been proposed that Arg 112 forms part of the electron transfer pathway in the CYP101·Pdx complex (*18*, *20*). We observe that the C helix and Cys 357 loop are affected by both Pdx and cytochrome b_5 and are likely sites for interaction with both proteins. One possible route for mechanical transmission of effector-induced perturbations from the proximal to distal side is via contacts between the C helix and the N-terminal region of the long I helix. A second route is via the irregular structure connecting the B′ and C helices. This connection is also close to the Cys 357 loop. Together, the two pathways bracket the heme and appear to be ideally situated to provide a "pincer" closure of the active site. Unfortunately, both the N-terminus of the I helix and the connection between helices B′ and C have proven to be difficult to assign, and until backbone resonances assignments are completed in these regions, these transmission pathways remain conjectural. As discussed above, the possibility that cytochrome b_5 may interact directly with the G helix cannot be discounted. However, such a binding mode would not seem to provide the mechanical stability needed to force closure or rearrangement of the substrate access channel.

Finally, the role of the high-barrier conformational shift observed in the active site of CYP101 upon addition of Pdx (*34*) in effector activity, if any, must be considered. While there is no direct evidence linking this conformational change to effector activity, we have recently found that in a mutant of CYP101, L358P, which exhibits many of the same spectral shifts as the Pdx−CYP−S−CO complex and has some constitutive camphor hydroxylation activity in the absence of Pdx (*38*), the camphor orientation is similar to that found in the Pdx^r−CYP−S−CO complex (that is, the conformation forced by Pdx binding) rather than that observed in wild-type CYP−S−CO alone (B. OuYang and S. Pochapsky, unpublished results). This indicates that the conformation required by the binding of Pdx^r to wild-type CYP−S−CO is stabilized in the absence of Pdx in the L358P mutant and suggests that the constitutive activity of the L358P mutant may be linked to this conformational change. If the high-barrier conformational change observed upon addition of Pdx in wild type CYP101 is essential for camphor hydroxylation (that is, if it is essential to effector activity), it is possible that a small fraction of the CYP101·cytochrome b_5 complex exists in this conformation, but the equilibrium constant for the conformational change is smaller than in the Pdx^r−CYP−S−CO complex and so is present to such a small extent that it is not readily detectable by NMR methods. A more complete analysis of NMR relaxation behavior of the CYP101−effector complex may provide insight into this possibility (*39*).

ACKNOWLEDGMENT

We are grateful to Luet-Lok Wong of Oxford University (Oxford, U.K.) for the pDNC334A plasmid that expresses CYP101 C334A and Prof. J. T. L. LeComte (Pennsylvania State University, University Park, PA) for the pETb5 plasmid that expresses the soluble domain of cytochrome b_5.

REFERENCES

1. Mueller, E. J., Loida, P. G., and Sligar, S. G. (1995) Twenty-five years of P450$_{cam}$ research, in *Cytochrome P450: Structure, Function and Biochemistry* (Ortiz de Montellano, P. R., Ed.) pp 83−124, Plenum Press, New York.
2. Denisov, I. G., Makris, T. M., Sligar, S. G., and Schlichting, I. (2005) Structure and chemistry of cytochrome P450, *Chem. Rev. 105*, 2253−2277.
3. Poulos, T. L., Finzel, B. C., and Howard, A. J. (1987) High-resolution crystal structure of cytochrome P450cam, *J. Mol. Biol. 195*, 687−700.
4. Peterson, J. A., and Graham-Lorence, S. E. (1995) Bacterial P450s: Structural similarity and functional differences, in *Cytochrome P450: Structure, Mechanism, and Biochemistry* (Ortiz de Montellano, P. R., Ed.) pp 151−179, Plenum Press, New York.
5. Brewer, C. B., and Peterson, J. A. (1988) Single turnover kinetics of the reaction between oxycytochrome P-450$_{cam}$ and reduced putidaredoxin, *J. Biol. Chem. 263*, 791−798.
6. Lipscomb, J. D., Sugar, S. G., Namtvedt, M. J., and Gunsalus, I. C. (1976) Autooxidation and hydroxylation reactions of oxygenated cytochrome P-450$_{cam}$, *J. Biol. Chem. 251*, 1116−1124.
7. Raag, R., Li, H., Jones, B. C., and Poulos, T. L. (1993) Inhibitor-induced conformational change in cytochrome P-450$_{CAM}$, *Biochemistry 32*, 4571−4578.
8. Raag, R., and Poulos, T. L. (1989) Crystal structure of the carbon monoxide-substrate-cytochrome P-450$_{CAM}$ ternary complex, *Biochemistry 28*, 7586−7592.
9. Schlichting, I., Berendzen, J., Chu, K., Stock, A. M., Maves, S. A., Benson, D. E., Sweet, R. M., Ringe, D., Petsko, G. A., and Sligar, S. G. (2000) The catalytic pathway of cytochrome P450$_{cam}$ at atomic resolution, *Science 287*, 1615−1622.
10. Jain, N. U., Tjioe, E., Savidor, A., and Boulie, J. (2005) Redox-dependent structural differences in putidaredoxin derived from homologous structure refinement via residual dipolar couplings, *Biochemistry 44*, 9067−9078.
11. Pochapsky, T. C., Jain, N. U., Kuti, M., Lyons, T. A., and Heymont, J. (1999) A refined model for the solution structure of oxidized putidaredoxin, *Biochemistry 38*, 4681−4690.
12. Pochapsky, T. C., Ye, X. M., Ratnaswamy, G., and Lyons, T. A. (1994) An NMR-derived model for the solution structure of oxidized putidaredoxin, a 2-Fe, 2-S ferredoxin from *Pseudomonas*, *Biochemistry 33*, 6424−6432.
13. Sevrioukova, I. F. (2005) Redox-dependent structural reorganization in putidaredoxin, a vertebrate-type [2Fe-2S] ferredoxin from *Pseudomonas putida*, *J. Mol. Biol. 347*, 607−621.
14. Sevrioukova, I. F., Garcia, C., Li, H., Bhaskar, B., and Poulos, T. L. (2003) Crystal structure of putidaredoxin, the [2Fe-2S] component of the P450$_{cam}$ monooxygenase system from *Pseudomonas putida*, *J. Mol. Biol. 333*, 377−392.
15. Hintz, M. J., Mock, D. M., Peterson, L. L., Tuttle, K., and Peterson, J. A. (1982) Equilibrium and kinetic studies of the interaction of cytochrome P-450$_{cam}$ and putidaredoxin, *J. Biol. Chem. 257*, 14324−14332.
16. Holden, M., Mayhew, M., Bunk, D., Roitberg, A., and Vilker, V. (1997) Probing the interactions of putidaredoxin with redox partners in camphor P450 5-monooxygenase by mutagenesis of surface residues, *J. Biol. Chem. 272*, 21720−21725.
17. Stayton, P. S., and Sligar, S. G. (1990) The cytochrome P-450$_{Cam}$ binding surface as defined by site-directed mutagenesis and electrostatic modeling, *Biochemistry 29*, 7381−7386.
18. Unno, M., Shimada, H., Toba, Y., Makino, R., and Ishimura, Y. (1996) Role of Arg^{112} of cytochrome P450$_{cam}$ in the electron transfer from reduced putidaredoxin. Analyses with site-directed mutants, *J. Biol. Chem. 271*, 17869−17874.

19. Pochapsky, T., Lyons, T., Kazanis, S., Arakaki, T., and Ratnaswamy, G. (1996) A structure-based model for cytochrome $P450_{cam}$-pufidaredoxin interactions, *Biochimie 78*, 723−733.
20. Roitberg, A. E., Holden, M. J., Mayhew, M. P., Kurnikov, I. V., Beratan, D. N., and Vilker, V. L. (1998) Binding and electron transfer between putidaredoxin and cytochrome $P450_{cam}$. Theory and experiments, *J. Am. Chem. Soc. 120*, 8927−8932.
21. Simonneaux, G., and Bondon, A. (2005) Mechanism of electron transfer in heme proteins and models: The NMR approach, *Chem. Rev. 105*, 2627−2646.
22. Pochapsky, S. S., Pochapsky, T. C., and Wei, J. W. (2003) A model for effector activity in a highly specific biological electron-transfer complex: The cytochrome $P450_{cam}$-putidaredoxin couple, *Biochemistry 42*, 5649−5656.
23. Shire, Y., Iizuka, T., Makino, R., Ishimura, Y., and Morishima, I. (1989) ^{15}N NMR study on cyanide ($C^{15}N$-) complex of cytochrome $P\text{-}450_{cam}$. Effects of *d*-camphor and putidaredoxin on the iron-ligand structure, *J. Am. Chem. Soc. 111*, 7707−7711.
24. Tosha, T., Yoshioka, S., Takahashi, S., Ishimori, K., Shimada, H., and Morishima, I. (2003) NMR study on the structural changes of cytochrome P450cam upon the complex formation with putidaredoxin: Functional significance of the putidaredoxin-induced structural changes, *J. Biol. Chem. 278*, 39809−39821.
25. Paine, M. J. I., Scrutton, N. S., Munro, A. W., Gutierrez, A., Roberts, G. C. K., and Wolf, C. R. (2005) Electron transfer partners of cytochrome P450, in *Cytochrome P450: Structure, Mechanism, and Biochemistry* (Ortiz de Montellano, P. R., Ed.) pp 115−148, Kluwer Academic/Plenum Publishers, New York.
26. Bridges, A., Gruenke, L., Chang, Y.-T., Vakser, I. A., Loew, G., and Waskell, L. (1998) Identification of the binding site on cytochrome P450 2B4 for cytochrome b_5 and cytochrome P450 reductase, *J. Biol. Chem. 273*, 17036−17049.
27. Stayton, P. S., Poulos, T. L., and Sligar, S. G. (1989) Putidaredoxin competitively inhibits cytochrome b5-cytochrome $P\text{-}450_{cam}$ association: A proposed molecular model for a cytochrome $P\text{-}450_{cam}$ electron-transfer complex, *Biochemistry 28*, 8201−8205.
28. Nickerson, D. P., and Wong, L.-L. (1997) The dimerization of *Pseudomonas putida* cytochrome $P450_{cam}$: Practical consequences and engineering of a monomeric enzyme, *Protein Eng. 10*, 1357−1361.
29. Gunsalus, I. C., and Wagner, G. C. (1978) Bacterial $P\text{-}450_{cam}$ methylene monooxygenase components: Cytochrome *m*, putidaredoxin, and putidaredoxin reductase, *Methods Enzymol. 52*, 166−187.
30. Von Bodman, S. B., Schuler, M. A., Jollie, D. R., and Sligar, S. G. (1986) Synthesis, bacterial expression, and mutagenesis of the gene coding for mammalian cytochrome b_5, *Proc. Natl. Acad. Sci. U.S.A. 83*, 9443−9447.
31. Pervushin, K., Riek, R., Wider, G., and Wüthrich, K. (1997) Attenuated T_2 relaxation by mutual cancellation of dipole−dipole coupling and chemical shift anisotropy indicates an avenue to NMR structures of very large biological macromolecules in solution, *Proc. Natl. Acad. Sci. U.S.A. 94*, 12366−12371.
32. Kay, L. E., Keifer, P., and Saarinen, T. (1992) Pure absorption gradient enhanced heteronuclear single quantum correlation spectroscopy with improved sensitivity, *J. Am. Chem. Soc. 114*, 10663−10665.
33. Palmer, A. G., III, Cavanagh, J., Wright, P. E., and Rance, M. (1991) Sensitivity improvement in proton-detected two-dimensional heteronuclear correlation NMR spectroscopy, *J. Magn. Reson. 93*, 151−170.
34. Wei, J. Y., Pochapsky, T. C., and Pochapsky, S. S. (2005) Detection of a high-barrier conformational change in the active site of cytochrome $P450_{cam}$ upon binding of putidaredoxin, *J. Am. Chem. Soc. 127*, 6974−6976.
35. Lüdemann, S. K., Lounnas, V., and Wade, R. C. (2000) How do substrates enter and products exit the buried active site of cytochrome P450cam? 2. Steered molecular dynamics and adiabatic mapping of substrate pathways, *J. Mol. Biol. 303*, 813−830.
36. Loida, P. J., and Sligar, S. G. (1993) Molecular recognition in cytochrome P-450: Mechanism for the control of uncoupling reactions, *Biochemistry 32*, 11530−11538.
37. Dunn, A. R., Dmochowski, I. J., Bilwes, A. M., Gray, H. B., and Crane, B. R. (2001) Probing the open state of cytochrome $P450_{cam}$ with ruthenium-linker substrates, *Proc. Natl. Acad. Sci. U.S.A. 98*, 12420−12425.
38. Tosha, T., Yoshioka, S., Ishimori, K., and Morishima, I. (2004) L358P mutation on cytochrome $P450_{cam}$ simulates structural changes upon putidaredoxin binding: The structural changes trigger electron transfer to oxy-$P450_{cam}$ from electron donors, *J. Biol. Chem. 279*, 42836−42843.
39. Millet, O., Loria, J. P., Kroenke, C. D., Pons, M., and Palmer, A. G. (2000) The static magnetic field dependence of chemical exchange linebroadening defines the NMR chemical shift time scale, *J. Am. Chem. Soc. 122*, 2867−2877.
40. Koradi, R., Billeter, M., and Wüthrich, K. (1996) MOLMOL: A program for display and analysis of macromolecular structures, *J. Mol. Graphics 14*, 51−55.

BI052318F